Improvements to laser wakefield accelerated electron beam stability, divergence, and energy spread using three-dimensional printed two-stage gas cell targets

M. Vargas, W. Schumaker, Z.-H. He, Z. Zhao, K. Behm, V. Chvykov, B. Hou, K. Krushelnick, A. Maksimchuk, V. Yanovsky, and A. G. R. Thomas

Articles you may be interested in

Measurements of high-energy radiation generation from laser-wakefield accelerated electron beamsa)
Phys. Plasmas **21**, 056704 (2014); 10.1063/1.4875336

High-quality electron beam from laser wake-field acceleration in laser produced plasma plumes
Appl. Phys. Lett. **102**, 231108 (2013); 10.1063/1.4810012

Generation of tunable, 100–800 MeV quasi-monoenergetic electron beams from a laser-wakefield accelerator in the blowout regimea)
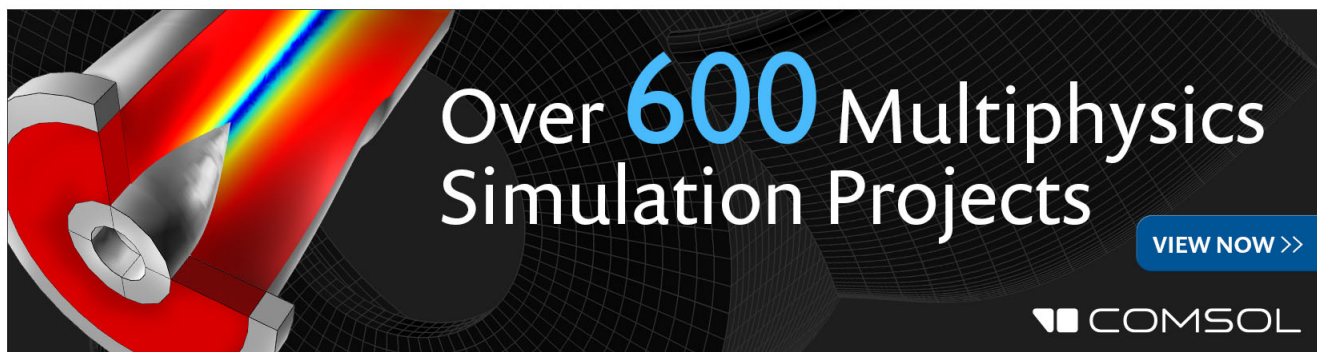Phys. Plasmas **19**, 056703 (2012); 10.1063/1.4718711

Laser wakefield acceleration of electron beams beyond 1 GeV from an ablative capillary discharge waveguide
Appl. Phys. Lett. **99**, 091502 (2011); 10.1063/1.3626042

On the stability of laser wakefield electron accelerators in the monoenergetic regimea)
Phys. Plasmas **14**, 056702 (2007); 10.1063/1.2436481

Improvements to laser wakefield accelerated electron beam stability, divergence, and energy spread using three-dimensional printed two-stage gas cell targets

M. Vargas, W. Schumaker, Z.-H. He, Z. Zhao, K. Behm, V. Chvykov, B. Hou, K. Krushelnick, A. Maksimchuk, V. Yanovsky, and A. G. R. Thomas[a]

Center for Ultrafast Optical Science, University of Michigan, Ann Arbor, Michigan 48109, USA

High intensity, short pulse lasers can be used to accelerate electrons to ultra-relativistic energies via laser wakefield acceleration (LWFA) [T. Tajima and J. M. Dawson, Phys. Rev. Lett. **43**, 267 (1979)]. Recently, it was shown that separating the injection and acceleration processes into two distinct stages could prove beneficial in obtaining stable, high energy electron beams [Gonsalves *et al.*, Nat. Phys. **7**, 862 (2011); Liu *et al.*, Phys. Rev. Lett. **107**, 035001 (2011); Pollock *et al.*, Phys. Rev. Lett. **107**, 045001 (2011)]. Here, we use a stereolithography based 3D printer to produce two-stage gas targets for LWFA experiments on the HERCULES laser system at the University of Michigan. We demonstrate substantial improvements to the divergence, pointing stability, and energy spread of a laser wakefield accelerated electron beam compared with a single-stage gas cell or gas jet target. © *2014 AIP Publishing LLC*. [http://dx.doi.org/10.1063/1.4874981]

Laser wakefield acceleration (LWFA) is a method of accelerating electrons to high energy using a high intensity laser coupled to plasma waves.[1] The laser pulse first ionizes the gas to produce a plasma. Electrons are subsequently expelled from the vicinity of the pulse due to the ponderomotive force of the laser. Ions, being much heavier than the electrons, are too slow to move on the time scale of the laser (30 fs), and therefore, a moving positive space charge is set up, the electric field of which can accelerate electrons behind it to ultra-relativistic energies.[5–7]

In practice, three types of targets have typically been used for LWFA: gas jets,[8] gas cells/capillary targets,[9] and pre ionized capillary targets.[10] The gas jet relies on supersonic flow through a conical nozzle to produce a uniform density. These devices are the least complicated and the easiest to align and operate, but the shot-to-shot reproducibility of the density profile may be limited. A gas cell consists of a large gas-filled cavity with a laser entrance and exit hole on either end. The advantage to using a gas cell lies in its ability to produce a very uniform density profile at low densities, and they have been shown to demonstrate increased stability.[11] Capillaries are long, narrow (100 μm diameter) cavities that may be etched into a Sapphire block, and filled with a gas. A discharge may be used to pre-ionize the plasma and generate a guiding density profile through thermal expansion.[10]

Precise control of the density profile of the gas in the interaction region is crucial for LWFA experiments. Typically, a high-density gas is desired for injecting the most charge into the wakefield for self injection.[12] However, at high densities the electron beams will quickly outrun the laser pulse, resulting in a process called dephasing where the electron beam begins to become decelerated by the reversed electric field of the wakefield. This process limits the maximum attainable electron energy. One way of overcoming

these competing requirements is to separate the injection and acceleration processes and to reduce the plasma density in the acceleration stage. Injection mechanisms include ionization induced injection,[13,14] using a second laser pulse,[15] and density ramp injection.[2,16] The requirements of these two competing processes, injection and acceleration, mandate some compromise with a uniform density gas target. However, by tailoring a 2 stage gas structure, the interaction can be separated specifically into an injection region—to trap charge in the wakefield—and an acceleration region—to maximize energy. Injection methods such as density gradients[2] and ionization injection[3,4] have been tried previously in two stage acceleration.

Using stereolithography three dimensional (3D) printing methods, in which a laser is used to cure individual layer of plastic so that features on the sub-100 μm scale are attainable, has previously been explored for producing gas nozzles for laser plasma applications.[17] For electron acceleration, the ability to build and test complex gas targets with a short turnaround provides a method for rapid improvements and high flexibility in gas target design. In this paper, we show that rapid prototyped two stage gas cell targets can be used for LWFA experiments and demonstrate improved divergence, pointing stability, and energy spread relative to our gas jet or single stage gas cell targets.

The experiments were performed using the HERCULES laser at the Center for Ultrafast Optical Science at the University of Michigan, a Ti:Sapphire laser with central wavelength of 810 nm, pulse duration of 35 fs, and with on-target power for these experiments ranging from 70 TW to 110 TW. The linearly polarized laser was focused using an *f*/20 off-axis paraboloidal mirror (2 m focal length) to a spot size of 22 μm, corresponding to a peak on-target intensity spanning $(6 - 9) \times 10^{18}$ W cm^{-2} (normalized vector potential of $a_0 = eE/m_e c\omega_0 = 1.7 - 2.1$). Typically, 27% of the laser energy is within the focal spot diameter. The laser pulse was incident on either a gas jet or gas cell of length

[a]Electronic mail: agrt@umich.edu

10 mm containing either helium gas or a premixed gas mixture of 2.5% nitrogen and 97.5% helium, with electron number densities measured by interferometry to be in the range $(0.3 - 1.0) \times 10^{19}$ cm^{-3}. The electron beam was deflected by a 0.75 T magnet onto a phosphor scintillating screen (LANEX regular), which was imaged using a charge coupled device camera to produce an energy spectrum in the horizontal direction and pointing and divergence information in the vertical direction.

Gas cell targets were designed using the Solidworks CAD package, and their performance was analyzed using the COMSOL Multiphysics computational fluid dynamics (CFD) platform.[22] After verifying the capability of the design, the gas cells were manufactured using the University of Michigan Medical Innovation Center's Viper SLA stereolithography 3D printer. In this system, a UV laser is focused into a tank of liquid photopolymer, curing a specific region of the photopolymer at each scanning location to solidify the plastic. Once the laser has scanned a specific layer, the build platform rises and the next cross-section can be cured. This device can achieve accuracies of approximately 100 μm in the horizontal plane and 20 μm in the vertical direction. Additionally, this system has been shown to produce rigid plastic structures that can hold densities well exceeding the desired operational pressures.[17] Our gas cells were compared with a standard gas jet design.[8] Fig. 1 shows the computer generated model of a 10 mm gas cell, along with photographs of new and used 3D-printed cells. After 500 shots at 100 TW (Fig. 1(c)), the plastic shows significant discoloration due to damage from scattered laser light, and a slightly enlarged entrance and exit hole (approximately 50% larger), but the gas cell is still useable.

The gas cells have a large base on which to mount a solenoid valve. When a pulse is sent to the solenoid valve, the reservoir of the gas cell is filled from the input to the base through six off-axis holes. A viewing window on either side is covered with a 1 mm thickness glass microscope slide cut to the appropriate size. The cells are designed such that the gas reaches an equilibrium in the cell thus producing a time-independent density profile. The inlet and outlet are sized to allow for the entrance and exit of the laser pulse while still maintaining the steady state flow and desired density profile.

A second design was a two stage gas cell (similar to Ref. 4), in which the gas type and density in each stage are independently controlled. The first stage is a 1 mm long "injector" stage with an input using a standard solenoid gas valve configuration at the bottom. The second stage is an 8 mm length "acceleration" stage with a separate input in the back of the cell. There is a separating wall of thickness 1 mm between the injector and accelerator stages. Holes of diameter 0.5 mm were made in both the outer walls and the separating wall for the two stage cell, which were aligned along the central axis to allow the laser to propagate through.

The expected density profile in the region between the two stages was studied using COMSOL CFD in order to verify that each stage provided individual control of the density across the path of the laser, since this region could not be optically probed. Simulations confirmed a steady state could be reached, so the gas cells could be pulsed without having to worry about timing jitter. By placing different backing pressures at each inlet of the gas cell, it is apparent that this two stage cell affords a significant amount of control over the density profile. However, it is important to note that there is some flow between the two stages, which means that each stage is not completely independent. This meant that the density in each stage has some dependency on the backing pressure in the other stage. To optimize injection and acceleration, a two-dimensional density scan was necessary. Fig. 2 shows how the average beam charge, peak energy, divergence, and deviation from center varied with the pressure in the two stages for a particular sized gas cell.

In these experiments, the targets investigated included: a 10 mm gas jet with either pure He or He with a 2.5% N_2 gas contaminant; a 10 mm single-stage gas cell emitting either pure He or He with a 2.5% N_2 gas contaminant; a two-stage gas cell, which contains He with a 2.5% N_2 gas contaminant in the "injection" stage and pure He in the "accelerator" stage.

Figure 3 shows an example series of consecutive scintillating screen images of the electron energy spectra under density optimized conditions for these different gas targets. The raw data highlight the typical improved stability in pointing, energy spread, peak energy, and divergence that the two-stage gas cell provides compared with the single stage gas targets. Figure 3(a) shows consecutive shots with a
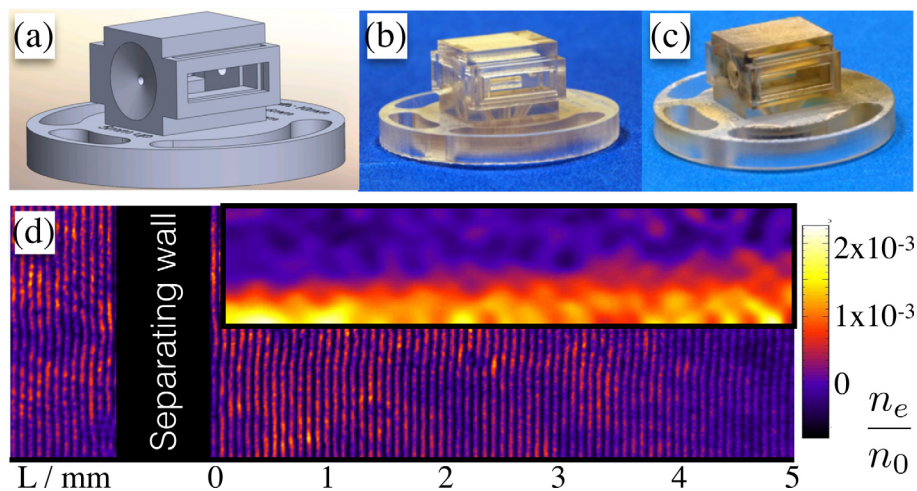

FIG. 1. (a) CAD model of 10 mm gas cell produced using solidworks, (b) unused gas cell, (c) gas cell after 500 shots at 100 TW laser power, and (d) interferogram of a two stage gas cell probed through the side windows. Inset panel shows the reconstructed plasma density profile after an 80 TW shot.
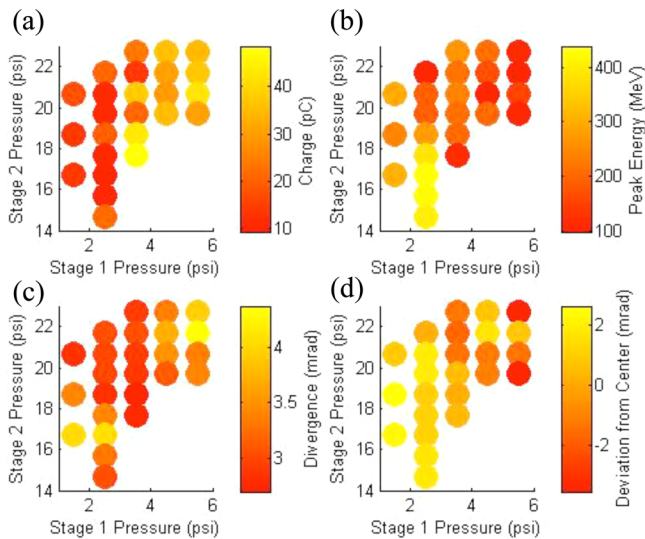
FIG. 2. Various average electron beam parameters as a function of backing pressure to the two feeds of the two-stage gas cell. (a) Charge, (b) peak energy, (c) beam divergence, and (d) deviation from center. Pressures are shown instead of densities because of the interdependency of the two compartments. With pressure supplied to one stage at a time, the interferometrically measured densities n are linearly dependent on the input pressure p. For stage 1, the relationship is $n = 1.2 \times 10^{18} \, cm^{-3} (p/psia)$ and for stage 2, the relationship is $n = 3.5 \times 10^{17} \, cm^{-3} (p/psia)$.

10 mm gas jet at 100 TW, displaying typical fluctuations of a long gas jet. Switching to the 10 mm single-stage gas cell with only 70 TW (Fig. 3(b)) shows improvements in peak energy, however, it also shows significant dephasing at this laser power (a lower laser power requires a higher optimal density and therefore a shorter dephasing length). This is remedied in Figure 3(c) by switching to the two-stage gas cell, producing electron beams with peak energies as high as 400 MeV, with significantly better stability. The same trend can be observed at higher laser power, with the two-stage cells providing consistently more stable electron beams at 110 TW and some control over the "dark current"[18] because of the injection only occurring in the first stage by tuning the density (Figs. 3(d) and 3(e)). In all the cases shown in Fig. 3, He was used as the gas medium, except for the two-stage gas cell where the acceleration stage was He but the injector was the He/N gas mixture.

To statistically study the comparative performance of a two-stage gas cell verses a single stage gas cell or a gas jet, a large quantity of data were collected and analyzed as a function of laser power. Fig. 4 shows a summary of various electron

beam parameters over a large data set with different gas targets, with each point representing a shot run of 48 shots on average. Although these data are averaged over shots at slightly different gas densities, in the range $(0.3 - 1.0) \times 10^{19} \, cm^{-3}$, the densities are all close to the threshold where electrons are generated, i.e., where the highest energy electrons are observed, depending on the laser power. Each point comprises the mean, maximum, root mean square (RMS) of that parameter taken for the entire density range of shots explored, which is more comprehensive than the representative shots shown in Fig. 2. These data are separated by target type and injection method (self-injection or ionization injection).

As can be seen from the data, the single-stage gas cells with ionization injection show the greatest overall beam charge, because they guide the laser pulse well, while continuously injecting charge throughout the entirety of the 10 mm cell (Fig. 4(a)), whereas the two-stage gas cell only traps charge in the injector stage. The charge measured from the gas jet is also lower than the single-stage gas cell even for ionization injection, which is likely to be related to the lower stability of the overall interaction relative to the gas cell. It is not altogether clear why the 10 mm gas jet does not show similar results to the 10 mm single stage gas cell. It may be related to the supersonic flow having significantly more stringent demands on manufacturing to prevent turbulent flow or hydrodynamic shocks. Alternatively, it may be that the shallow density ramp interface of the gas cell is beneficial to the laser propagation.

The gas jets tend to achieve lower peak energies, which is also likely to be related to the instability of the electrons generated by the supersonic nozzle at the 10 mm length. The two-stage and single-stage cell show similar peak energies, which is expected as the electrons are accelerated over similar distances and the gas flow is similar. A significant improvement is the reduced energy spread of the electron beam from the two-stage gas cells relative to the other targets, which is clearly due to the separation of the injection and acceleration processes and is related to the lower charge observed. If too much charge is trapped in the wakefield, it will significantly modify the field structure.[19] In addition, continuous injection will evidently result in a large energy spread.

The pointing stability is clearly improved for the gas cell targets relative to the gas jet, which is likely to be related to the other improved characteristics such as the peak energy. The divergence of beams from the single-stage gas
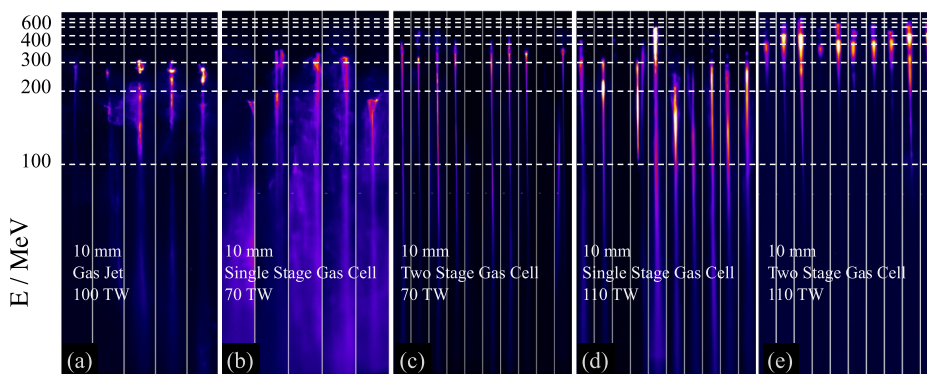

FIG. 3. Series of consecutive scintillating screen images showing electron energy spectra under density optimized conditions for acceleration in pure He gas for a (a) 10 mm gas jet for $P_L = 100$ TW, (b) 10 mm single-stage gas cell for $P_L = 70$ TW, (c) 10 mm two-stage gas cell for $P_L = 70$ TW, (d) 10 mm single-stage gas cell with $P_L = 110$ TW, and (e) 10 mm two-stage gas cell with $P_L = 110$ TW. For the two-stage gas cell, the first stage contains a 2.5% N contaminant.
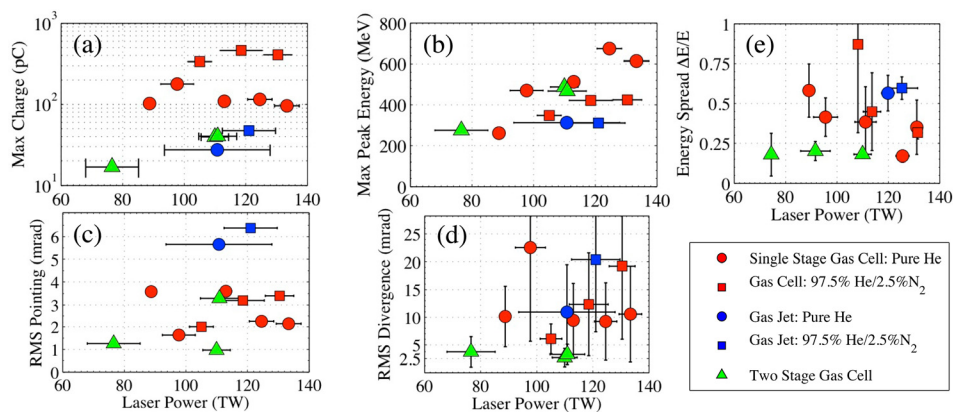
FIG. 4. Various electron beam parameters compiled for large data sets (on average 48 shots per datum) with different gas targets: (a) Maximum charge (logarithmic), (b) maximum *peak* energy, (c) RMS pointing, (d) RMS divergence, and (e) average $\Delta E/E$ for best three consecutive shots in each run.

cell and the gas jet are similar, indicating that this may be more related to the increased charge trapped relative to the two-stage gas cell. By controlling the charge injected, the RMS beam divergence produced by the two-stage gas cell is comparable to reported results for electrons beams generated in capillary guided LWFA.[20] The best pointing stability of the gas is also similar to the results from capillary waveguides.

We have shown that rapid prototyping using stereolithography based 3D printing can produce gas cell targets which demonstrate significant improvements in charge, stability, and maximum energy of the output electron beams compared with our supersonic gas jet. A single-stage gas cell with ionization injection can be implemented for high beam charge applications. We have shown that the two-stage gas cell shows an additional improvement over our single-stage gas cell and gas jet targets in terms of energy spread, divergence, and pointing stability. Because of the flexibility and cost effectiveness of the rapid prototyping process, variable length gas cells, or more complex staged structures may easily be produced for laser-plasma interactions. In addition, applications for LWFA such as phase contrast imaging using the betatron x-rays[21] require energy and pointing stability of electron beam as well as a small x-ray source size.

[1]T. Tajima and J. M. Dawson, Phys. Rev. Lett. **43**, 267 (1979).

[2]A. J. Gonsalves, K. Nakamura, C. Lin, D. Panasenko, S. Shiraishi, T. Sokollik, C. Benedetti, C. B. Schroeder, C. G. R. Geddes, J. van Tilborg, J. Osterhoff, E. Esarey, C. Toth, and W. P. Leemans, Nat. Phys. **7**, 862 (2011).

[3]J. S. Liu, C. Q. Xia, W. T. Wang, H. Y. Lu, Ch. Wang, A. H. Deng, W. T. Li, H. Zhang, X. Y. Liang, Y. X. Leng, X. M. Lu, C. Wang, J. Z. Wang, K. Nakajima, R. X. Li, and Z. Z. Xu, Phys. Rev. Lett. **107**, 035001 (2011).

[4]B. B. Pollock, C. E. Clayton, J. E. Ralph, F. Albert, A. Davidson, L. Divol, C. Filip, S. H. Glenzer, K. Herpoldt, W. Lu, K. A. Marsh, J. Meinecke, W. B. Mori, A. Pak, T. C. Rensink, J. S. Ross, J. Shaw, G. R. Tynan, C. Joshi, and D. H. Froula, Phys. Rev. Lett. **107**, 045001 (2011).

[5]S. P. D. Mangles, C. D. Murphy, Z. Najmudin, A. G. R. Thomas, J. L. Collier, A. E. Dangor, E. J. Divall, P. S. Foster, J. G. Gallacher, C. J. Hooker, D. A. Jaroszynski, A. J. Langley, W. B. Mori, P. A. Norreys, F. S. Tsung, R. Viskup, B. R. Walton, and K. Krushelnick, Nature (London) **431**, 535 (2004).

[6]C. G. R. Geddes, C. Toth, J. v. Tilborg, E. Esarey, C. B. Schroeder, D. Bruhwiler, C. Nieter, J. Cary, and W. P. Leemans, Nature (London) **431**, 538 (2004).

[7]J. Faure, Y. Glinec, A. Pukhov, S. Kiselev, S. Gordienko, E. Lefebvre, J.-P. Rousseau, F. Burgy, and V. Malka, Nature (London) **431**, 541 (2004).

[8]S. Semushin and V. Malka, Rev. Sci. Instrum. **72**, 2961 (2001).

[9]W. P. Leemans, B. Nagler, A. J. Gonsalves, Cs. Tóth, K. Nakamura, C. G. R. Geddes, E. Esarey, C. B. Schroeder, and S. M. Hooker, Nat. Phys. **2**, 696 (2006); K. Nakamura, B. Nagler, Cs. Tóth, C. G. R. Geddes, C. B. Schroeder, E. Esarey, W. P. Leemans, A. J. Gonsalves, and S. M. Hooker, Phys. Plasmas **14**, 056708 (2007).

[10]D. J. Spence and S. M. Hooker, Phys. Rev. E **63**, 015401(R) (2000); D. J. Spence, A. Butler, and S. M. Hooker, J. Opt. Soc. Am. B **20**, 138 (2003); S. Karsch, J. Osterhoff, A. Popp, T. P. Rowlands-Rees, Zs. Major, M. Fuchs, B. Marx, R. Hörlein, K. Schmid, L. Veisz, S. Becker, U. Schramm, B. Hidding, G. Pretzler, D. Habs, F. Grüner, F. Krausz, and S. M. Hooker, New J. Phys. **9**, 415 (2007).

[11]J. Osterhoff, A. Popp, Zs. Major, B. Marx, T. P. Rowlands-Rees, M. Fuchs, M. Geissler, R. Hrlein, B. Hidding, S. Becker, E. A. Peralta, U. Schramm, F. Grüner, D. Habs, F. Krausz, S. M. Hooker, and S. Karsch, Phys. Rev. Lett. **101**, 085002 (2008).

[12]D. H. Froula, C. E. Clayton, T. Dppner, K. A. Marsh, C. P. J. Barty, L. Divol, R. A. Fonseca, S. H. Glenzer, C. Joshi, W. Lu, S. F. Martins, P. Michel, W. B. Mori, J. P. Palastro, B. B. Pollock, A. Pak, J. E. Ralph, J. S. Ross, C. W. Siders, L. O. Silva, and T. Wang, Phys. Rev. Lett. **103**, 215006 (2009); S. P. D. Mangles, G. Genoud, M. S. Bloom, M. Burza, Z. Najmudin, A. Persson, K. Svensson, A. G. R. Thomas, and C.-G. Wahlstrm, Phys. Rev. ST-Accel. Beams **15**, 011302 (2012).

[13]A. Pak, K. A. Marsh, S. F. Martins, W. Lu, W. B. Mori, and C. Joshi, Phys. Rev. Lett. **104**, 025003 (2010).

[14]C. McGuffey, A. G. R. Thomas, W. Schumaker, T. Matsuoka, V. Chvykov, F. J. Dollar, G. Kalintchenko, V. Yanovsky, A. Maksimchuk, K. Krushelnick, V. Yu. Bychenkov, I. V. Glazyrin, and A. V. Karpeev, Phys. Rev. Lett. **104**, 025004 (2010).

[15]J. Faure, C. Rechatin, A. Norlin, A. Lifschitz, Y. Glinec, and V. Malka, Nature **444**, 737–739 (2006); A. G. R. Thomas, C. D. Murphy, S. P. D. Mangles, A. E. Dangor, P. Foster, J. G. Gallacher, D. A. Jaroszynski, C. Kamperidis, K. L. Lancaster, P. A. Norreys, R. Viskup, K. Krushelnick, and Z. Najmudin, Phys. Rev. Lett. **100**, 255002 (2008); H. Kotaki, I. Daito, M. Kando, Y. Hayashi, K. Kawase, T. Kameshima, Y. Fukuda, T. Homma, J. Ma, L.-M. Chen, T. Zh. Esirkepov, A. S. Pirozhkov, J. K. Koga, A. Faenov, T. Pikuz, H. Kiriyama, H. Okada, T. Shimomura, Y. Nakai, M. Tanoue, H. Sasao, D. Wakai, H. Matsuura, S. Kondo, S. Kanazawa, A. Sugiyama, H. Daido, and S. V. Bulanov, *ibid.* **103**, 194803 (2009).

[16]H. Suk, N. Barov, J. B. Rosenzweig, and E. Esarey, Phys. Rev. Lett. **86**, 6, 1011 (2001); S. Kalmykov, S. A. Yi, V. Khudik, and G. Shvets, *ibid.* **103**, 135004 (2009); C. G. R. Geddes, K. Nakamura, G. R. Plateau, Cs. Toth, E. Cormier-Michel, E. Esarey, C. B. Schroeder, J. R. Cary, and W. P. Leemans, *ibid.* **100**, 215004 (2008); A. Buck, J. Wenz, J. Xu, K. Khrennikov, K. Schmid, M. Heigoldt, J. M. Mikhailova, M. Geissler, B. Shen, F. Krausz, S. Karsch, and L. Veisz, *ibid.* **110**, 185006 (2013).

[17]S. W. Jolly, Z. He, C. McGuffey, W. Schumaker, K. Krushelnick, and A. G. R. Thomas, Rev. Sci. Instrum. **83**, 073503 (2012).

[18]S. Y. Kalmykov, A. Beck, X. Davoine, E. Lefebvre, and B. A. Shadwick, New J. Phys. **14**, 033025 (2012).

[19]M. Tzoufras, W. Lu, F. S. Tsung, C. Huang, W. B. Mori, T. Katsouleas, J. Vieira, R. A. Fonseca, and L. O. Silva, Phys. Rev. Lett. **101**, 145002 (2008).

[20]P. A. Walker, N. Bourgeois, W. Rittershofer, J. Cowley, N. Kajumba, A. R. Maier, J. Wenz, C. M. Werle, S. Karsch, F. Grner, D. R. Symes,

P. P. Rajeev, S. J. Hawkes, O. Chekhlov, C. J. Hooker, B. Parry, Y. Tang, and S. M. Hooker, New J. Phys. **15**, 045024 (2013).

[21]A. Rousse, K. T. Phuoc, R. Shah, A. Pukhov, E. Lefebvre, V. Malka, S. Kiselev, F. Burgy, J.-P. Rousseau, D. Umstadter, and D. e. Hulin, Phys. Rev. Lett. **93**, 135005 (2004); S. Kneip, C. McGuffey, J. L. Martins, S. F. Martins, C. Bellei, V. Chvykov, F. Dollar, R. Fonseca, C. Huntington, G. Kalintchenko, A. Maksimchuk, S. P. D. Mangles, T. Matsuoka, S. R. Nagel, C. A. J. Palmer, J. Schreiber, K. Ta Phuoc, A. G. R. Thomas, V. Yanovsky, L. O. Silva, K. Krushelnick and Z. Najmudin, Nat. Phys. **6**, 980 (2010).

[22]See comsol.com for information about the COMSOL CFD code.